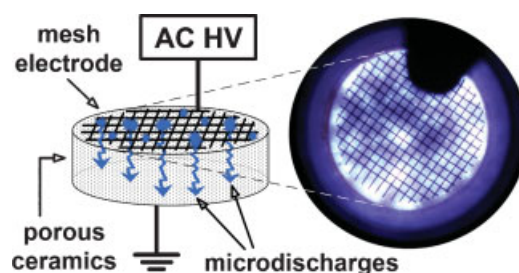


# Electrical and Optical Properties of AC Microdischarges in Porous Ceramics

Karol Hensel,\* Viktor Martišovič, Zdenko Machala, Mário Janda, Michal Leštinský, Pierre Tardiveau, Akira Mizuno

Generation of microdischarges inside porous ceramics by AC high voltage was explored. The physical properties of the microdischarges were investigated by electrical measurements, photographic visualization, and optical emission spectroscopy. The effects of pore size, discharge power, and gas mixture composition on the discharge properties and its development are described. The optimum generation and distribution of the microdischarges was observed with pore sizes of 50 and 80  $\mu\text{m}$ . The emission spectra of the microdischarges indicated their strongly non-equilibrium character. A theoretical analysis of the microdischarge mechanism is provided, accounting for the pore size and the elementary processes such as ionization, recombination, and ambipolar diffusion.



## Introduction

Research of various types of non-thermal plasmas generated by electrical discharges at atmospheric pressure has undergone fast development in the past two decades. Streamer and pulsed coronas, and various types of dielectric or ferroelectric barrier discharges are mostly investigated and used for applications. They are typical with a large number of thin filamentary channel, called microdischarges. The microdischarges produce a high density of energetic electrons and free radicals at relatively low energy consumption and so they represent a potential method for flue gas treatment.<sup>[1–3]</sup> The efficiency of the

treatment effect can be enhanced when the discharge plasma is combined with a catalyst. The catalyst, typically of the ferroelectric pellet bed type or of honeycomb structure, can be placed either behind the plasma zone or directly in it.<sup>[4–7]</sup> The small volume of the generated plasma and the pressure drop on the catalyst associated with the pellet bed type plasma reactors lead to more prospective uses of porous materials, such as honeycomb monoliths or porous ceramics.

In recent years, a few pioneering works have appeared dealing with the generation of microdischarges in narrow cavities and capillaries of porous dielectric materials.<sup>[8–10]</sup> The objectives of these studies were to investigate the physical properties of the microdischarges and to use them for the removal of volatile organic compounds and nitrogen oxides. Unlike most pulsed discharges that need special high voltage power supplies generating pulses with a rise time of some tens of nanoseconds in order to efficiently produce radicals and oxidants, microdischarges can be generated with an AC or a DC high voltage power supply.<sup>[11–13]</sup> This fact substantially enlarges the possibilities for microdischarge use in porous materials because high investment costs for the construction of a pulsed power supply are reduced.

K. Hensel, V. Martišovič, Z. Machala, M. Janda, M. Leštinský  
Department of Astronomy, Earth Physics and Meteorology,  
Faculty of Mathematics, Physics and Informatics, Comenius  
University, 84248 Bratislava, Slovakia

E-mail: hensel@fmph.uniba.sk

P. Tardiveau

Laboratoire de Physique des Gaz et des Plasmas, Université  
Paris-Sud, 91400 Orsay, France

A. Mizuno

Department of Ecological Engineering, Toyohashi University of  
Technology, 441858 Toyohashi, Japan

The objective of this study was to investigate the physical properties of the microdischarges generated inside porous ceramics by AC high voltage. The study follows the previous works that described the properties of the microdischarges generated by DC power.<sup>[11,12]</sup> The methods of the investigations in the presented work consist of electrical and optical measurements to determine the optimal conditions for discharge generation with respect to pore size, discharge power, gas mixture composition, and gas flow rate. The experimental measurements are supplemented with a theoretical analysis of the microdischarge mechanism with respect to the elementary processes including ionization, recombination, and ambipolar diffusion.

## Experimental Part

The experimental setup including a discharge reactor and electrical and optical circuits is depicted in Figure 1. The discharge reactor consisted of a porous ceramic placed between two stainless steel mesh electrodes inside the quartz cylinder. The ceramics were composed of mainly alumina or fused silica, and their diameter and thickness were 31 and 7 mm, respectively. The pore sizes of the ceramics were 2, 10, 30, 50, 80, 120, and 200  $\mu\text{m}$ . The whole reactor was placed in a Faraday cage to reduce induced noise signals and to allow correct measurement of voltage and current waveforms.

An AC regulated high voltage power supply (50 Hz) connected via a 5-M $\Omega$  series resistor limiting the total current was used to generate the discharge. The voltage on the reactor was measured by a high voltage probe (Tektronix P6015A) and the discharge current was measured using a current probe (Pearson Electronics 2877;  $1 \text{ V} \cdot \text{A}^{-1}$ ), both linked to the digitizing oscilloscope (Tektronix TDS2024; 200 MHz,  $2.5 \text{ GS} \cdot \text{s}^{-1}$ ). The total power including power losses in the electrical circuit (e.g., in transformer windings and serial resistance) was measured by a digital wattmeter (Metex

3860M). The net discharge power was determined by subtracting the power consumed in the circuit without the reactor (no-load conditions) from the total power.

An optical emission spectroscopy system consisted of a dual fiber-optic compact spectrometer (Ocean Optics SD2000) with a charge-coupled device (CCD) detector used for fast scanning in the ultraviolet (UV; 200–500 nm) and visible-near infrared (VIS-NIR; 400–1 050 nm) regions, with spectral resolutions of 0.6 and 1.2 nm, respectively. The spectrometer recorded the light emission integrated from the whole surface of the ceramics. Photographs of discharge were taken with a digital camera (Nikon E4300) with manually adjustable aperture and exposure time.

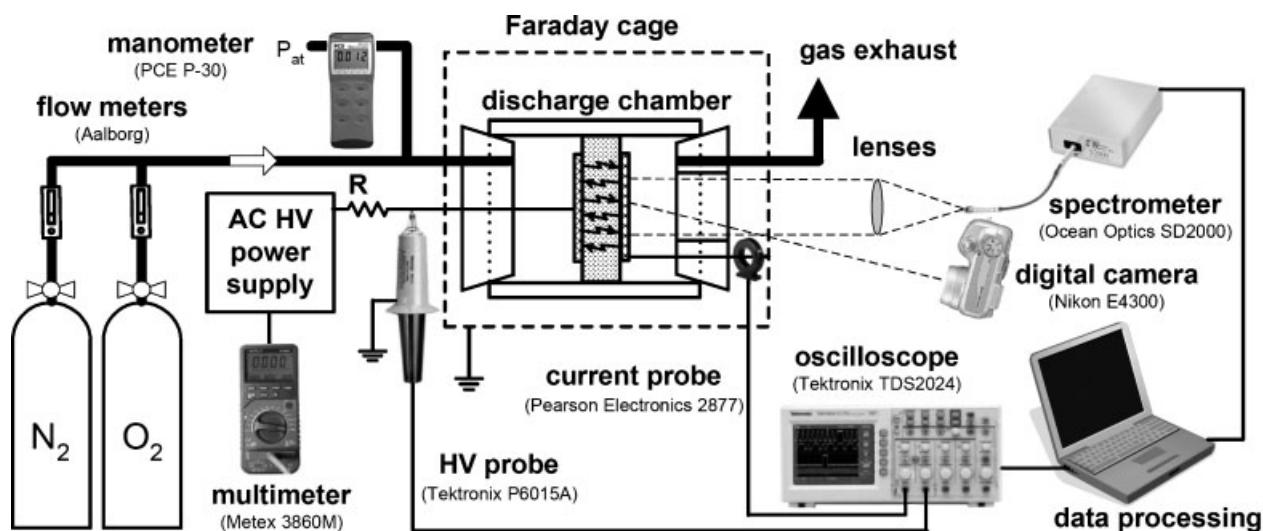
All experiments were carried out in mixtures of nitrogen and oxygen at atmospheric pressure and at room temperature. The total gas flow rate ranged from 0.4 to  $2 \text{ L} \cdot \text{min}^{-1}$ . The pressure drop across the discharge reactor was measured with a digital manometer (PCE P-30).

## Results and Discussion

The physical properties of the microdischarges were investigated by electrical measurements, photographic visualization, and optical emission spectroscopy. These results are separated in the three following sections. The theoretical part in the next section analyses the microdischarge mechanism. Finally, in the last section, we address some technical issues such as pressure drop and plasma-surface interaction.

### 1. Electrical Characteristics

In the previous studies investigating DC-driven microdischarges, we found that the successful generation of microdischarges inside the ceramics depended on the pore size and the applied voltage.<sup>[11,12]</sup> We reported that at



■ Figure 1. Schematic of the experimental system.

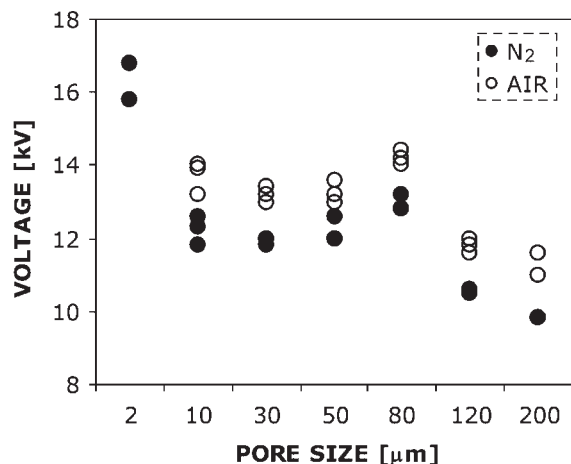


Figure 2. Onset voltage of the capillary microdischarges in N<sub>2</sub> and in 20% O<sub>2</sub> in N<sub>2</sub>.

small voltage, a surface discharge could be observed, especially with the ceramics of the smallest pore size. With increased applied voltage, a gradual change of the discharge mode was observed. At a specific voltage, the charges of the surface discharge enter the ceramics and capillary discharges (microdischarges) are formed inside it. Similar effects also apply when using AC power.

Figure 2 shows the amplitude of the AC applied voltage at the moment of the barrier discharge transition to the capillary microdischarges inside the ceramics. As can be seen, the onset voltage of the microdischarges increased with decreasing pore size, in particular for pore sizes less than several micrometers, and also increased with the oxygen contents. The barrier discharge mode was dominant in the ceramics with the smallest pore size ( $\leq 2 \mu\text{m}$ ). For these ceramics, an extreme increase of the voltage would be required to obtain the microdischarges. We have measured power-to-voltage ( $P/U$ ) characteristics of the discharges. The characteristics of the barrier discharge were almost identical for all ceramics. While barrier discharge is a low-energy discharge that spreads into a larger surface discharge at the dielectric surface, the capillary microdischarge mode is, on the contrary, a very short spark breakdown, which carries substantially more energy in one pulse. Therefore, upon the transition of the barrier discharge into the microdischarges, the slope of the  $P/U$  curve increased. Figure 3 displays the  $P/U$  characteristics after the onset of the microdischarges in three different ceramics. While the slope of the barrier discharge characteristics was independent of the ceramics used, the  $P/U$  slope of the microdischarge characteristics increased with the pore size. The pore size determined the volume of the discharge and thus limited the discharge current. The increase of the slope at the constant voltage was the result of the increase of the discharge current. The  $P/U$  slope also

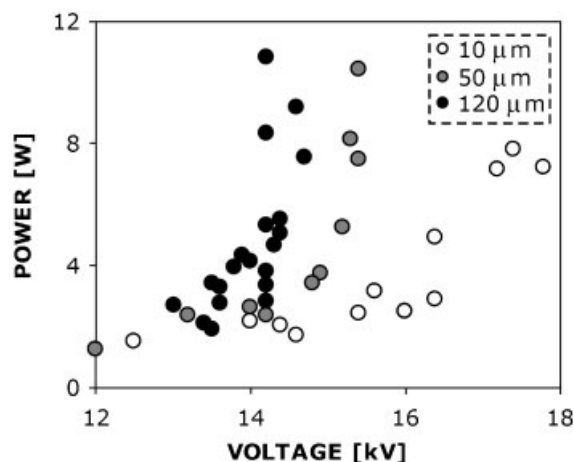


Figure 3. Discharge power as a function of the applied voltage (20% O<sub>2</sub> in N<sub>2</sub>).

increased with the content of nitrogen in the gas mixture. This is due to the increased number and homogeneity of distribution of discharge channels in the ceramics, which are explained later in this paper.

We recorded oscilloscopic waveforms of the applied voltage and the current pulses for both the barrier discharge and the capillary microdischarges. Figure 4 presents the typical waveforms obtained at various timescales. The discharges occurred both in negative and positive polarity of the applied voltage. During one cycle, several discharges occurred and their number increased with the applied voltage. The barrier discharge typically showed short pulses of amplitudes of several tenths of milliamperes with insignificant voltage drop during the pulse. On the other hand, the capillary microdischarges were accompanied by sharp current pulses and significant voltage drop to almost zero. The pulses had a short duration of less than 100 ns, repetition rates of 1–10 kHz, and amplitudes reaching several tenths of amperes; that is, three orders of magnitude higher than the barrier discharge. As Figure 5 shows, the amplitude of the microdischarge pulse generally increased with the applied voltage and the pore size.

The pore size determined the onset voltage of the microdischarges and also the diameter of the discharge channels. Inside bigger pores, channels with bigger diameters can develop. At a given voltage, the larger channel can carry bigger discharge currents in the pulses with correspondingly higher amplitudes. Figure 6 shows the pulse amplitude as a function of the pore size for a given constant power. The figure shows two data series, one for a constant discharge power of 2.5 W (corresponding total powers were 24–28 W) and the other one for a constant total power of 28 W (discharge powers were 2.5–8 W). The amplitude of the pulses increased with the pore size

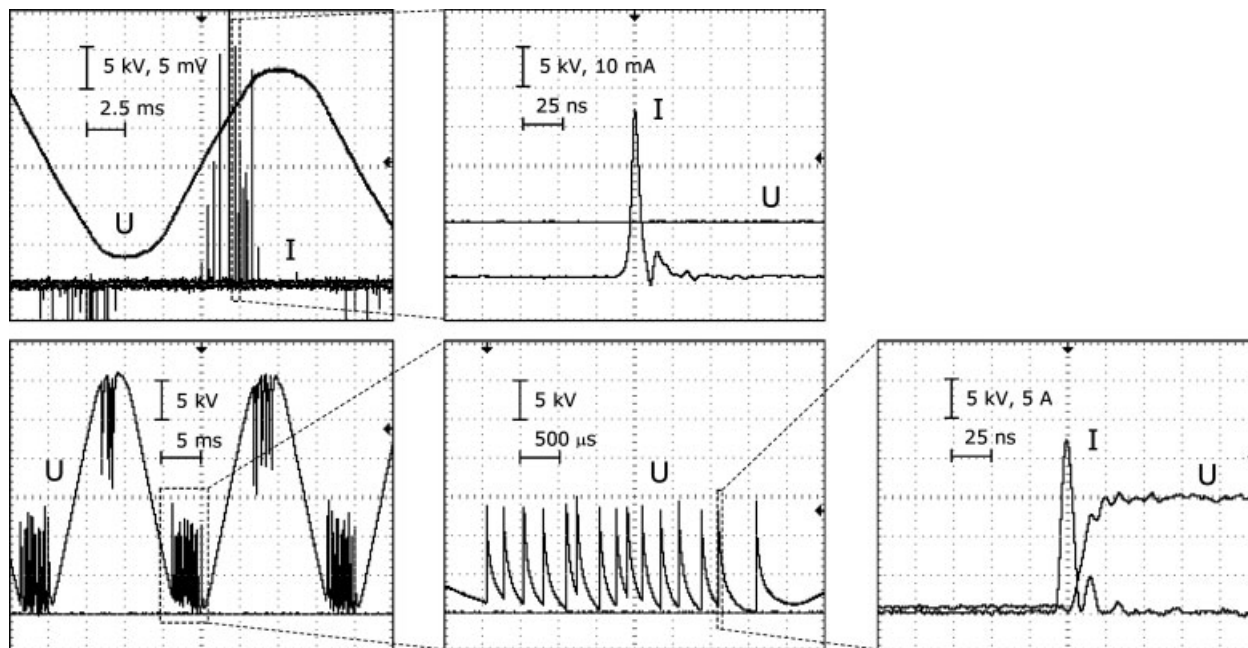


Figure 4. Voltage and current waveforms of the barrier discharge (upper row,  $U = 12.2$  kV,  $P = 0.1$  W) and the capillary microdischarges (lower row,  $U = 16.2$  kV,  $P = 6.7$  W) in porous ceramics at different timescales (pore size  $30 \mu\text{m}$ , 20%  $\text{O}_2$  in  $\text{N}_2$ ).

and then decreased slightly for the biggest pores sizes. As the discharge power and current at a given voltage are the highest for the biggest pores, it is possible that the frequency of the pulses may play an important role. Additional investigations are, however, needed to clarify this problem.

Regarding the gas composition, the amplitude of the pulses increased with the oxygen contents, which is related to either constant applied voltage or discharge power. On the other hand, an increase of the oxygen contents caused a reduction of the total number of discharge channels.

Thus, the mean discharge current/power at a given voltage decreased.

## 2. Photographic Visualization

Photographic documentation and optical emission spectroscopy of the discharges were performed simultaneously with the electrical measurements. The photographs were recorded to visualize the macroscopic character and spatial development of the discharge, depending on the discharge power, the gas composition, the pore size, and the discharge

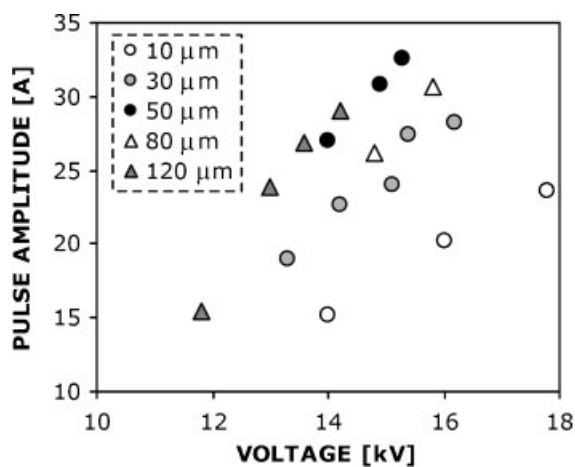


Figure 5. Current pulse amplitude as a function of the applied voltage (20%  $\text{O}_2$  in  $\text{N}_2$ ).

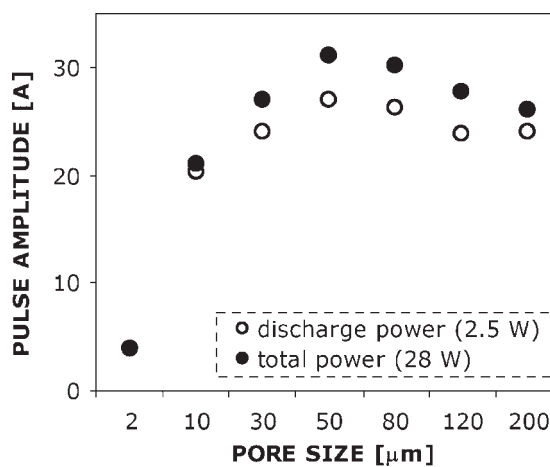
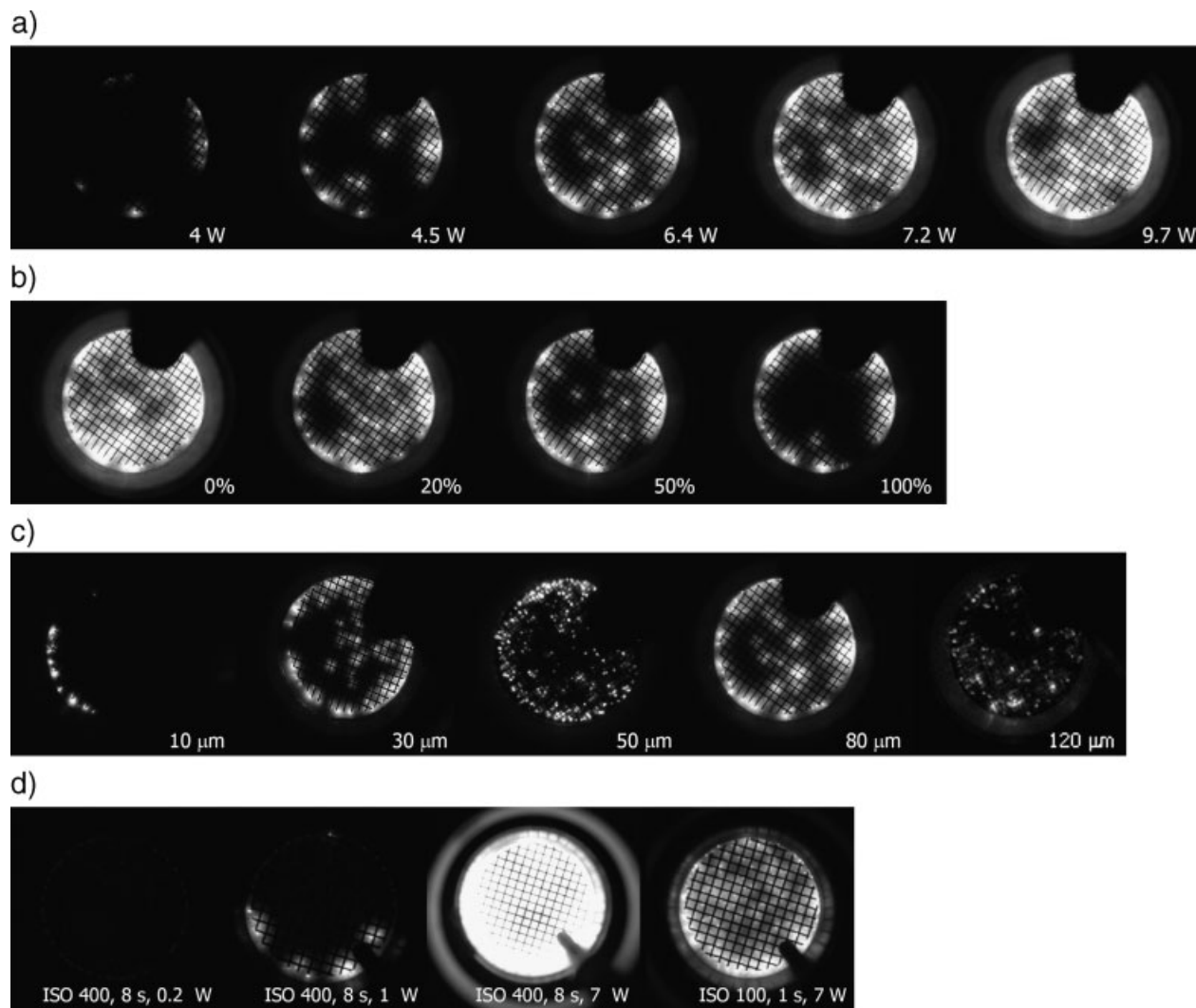


Figure 6. Current pulse amplitude as a function of the pore size (20%  $\text{O}_2$  in  $\text{N}_2$ ).



**Figure 7.** (a) Effect of discharge power (pore size  $80\ \mu\text{m}$ , ISO 100, exposure time 1 s, 20%  $\text{O}_2$  in  $\text{N}_2$ ). (b) Effect of oxygen content (pore size  $80\ \mu\text{m}$ , ISO 100, exposure time 1 s,  $P \approx 7\ \text{W}$ ). (c) Effect of pore size (ISO 100, exposure time 1 s,  $P = 6.4\ \text{W}$ , 20%  $\text{O}_2$  in  $\text{N}_2$ ). (d) Comparison of the barrier discharge (two photographs on left) and the microdischarges (two photographs on right). The first three photographs (from left) were taken with enhanced sensitivity and exposure time (pore size  $80\ \mu\text{m}$ ,  $\text{N}_2$ ).

mode. All photographs were taken from the direction perpendicular to the ceramics surface; however, we also observed a light emission along the side of the ceramics. These lateral observations indicated that microdischarges occur inside the ceramics and not only between the mesh electrode and the ceramics surface.

Observations of the microdischarges showed that the spatial and temporal distribution of the channels was not steady but changed randomly. Figure 7a–c shows three sets of photographs visualizing the effects of the power, the gas composition, and the pore size on the macroscopic character of microdischarges and their spatial distribution. All photographs were taken with the same sensitivity and time exposure. The intensity of the light emission

increased with the discharge power resulting from the increase of the number of discharge channels and the discharge current (Figure 7a). It is also evident that the increase of the oxygen contents in the gas mixture resulted in the redistribution of the microdischarge channels inside the ceramics. In nitrogen, the light emission was distributed in a relatively homogenous fashion over the entire surface of the ceramics. With the increase of oxygen in the mixtures, a gradual migration of the channels toward the edge of the ceramics occurred (Figure 7b). In pure oxygen, the channels concentrated mostly around the outer circumference of the mesh electrodes and there was almost no visible emission in the center of the ceramics. The increase of oxygen also

caused a reduction of the total number of discharge channels, which resulted in a decrease of the mean discharge current/power at a given voltage.

The reason why the microdischarges in oxygen-containing mixtures are more likely to occur mainly at the circumference of the mesh is the higher electric field at the electrode edges. When the mixture contains oxygen, which is an electronegative gas, the breakdown voltage increased due to the loss of electrons by attachment. This was confirmed by the measurements of the breakdown voltage documented in Figure 2. Therefore, for the same applied voltage, the breakdown is easier in nitrogen than in oxygen, resulting in preferential appearance of discharges at the edges (in the stronger fields) in oxygen-containing mixtures. In addition, the amplitudes of the current pulses were higher in oxygen-containing mixtures. Once the breakdown occurs at the edges, the current pulses become stronger there than in nitrogen, and so does the light intensity. This even strengthens the effect of dominant discharge appearance at the edges in oxygen-containing mixtures.

Comparing the ceramics for a given power and gas mixture, the most homogenous distribution of the channels inside the ceramics was observed for the pore sizes of 50 and 80  $\mu\text{m}$  (Figure 7c). Increasing the pore size and the applied voltage, the number and the intensity of the microdischarges increased and the homogeneity of their distribution and the light emission improved. However, for the biggest pore size, a chance that one or several channels suddenly become more intense than the others also increased. For 200- $\mu\text{m}$  ceramics, such channels were observed very soon after the microdischarge onset. With increasing applied voltage, the intensity of such channels increased more rapidly than that of other channels, and the overall homogeneity of the light emission was worse. The different character of the photographs for 50 and 120- $\mu\text{m}$  ceramics compared with the others is, however, due to the color of the ceramics. The ceramics were dominantly composed of  $\text{Al}_2\text{O}_3/\text{SiO}_2$  mixture, but to achieve desired pores sizes during manufacturing, various admixtures and sintering process conditions were used. The processing of the ceramics affected their color, which was dark (brown and black) for 50 and 120  $\mu\text{m}$ , compared to white for the others. As a result, the discharge in the dark ceramics appears different.

We also took photographs of the barrier discharge mode. Figure 7d shows the set of four photographs of both the barrier discharge and the microdischarge modes. The first photograph in Figure 7d presents the light emission of the barrier discharge at a power of 0.1 W. Compared to previous photographs, the sensitivity of the camera had to be increased to ISO 400 and the exposure time to 8 s to be able to record any light from the barrier discharge. The second photograph shows the discharge at the moment of

the transition in the microdischarges (bright spots), which occurred at a power of about 1 W. The intensity of these microdischarges was much stronger compared to the diffuse light of the barrier discharge. In the third photograph, the light of fully developed microdischarges can be seen. The photograph is overexposed because it was taken with the same sensitivity and exposure as the previous two photographs. The last photograph shows the same discharge with the sensitivity and exposure decreased to a "standard level" (ISO 100, 1 s), the same as for all other photographs in Figure 7a–c. Figure 7d clearly shows that the light intensity of the barrier discharge was much smaller than that of the microdischarges. The contribution of the barrier discharges to the appearance of the photographs with many microdischarge channels is therefore very limited. We may assume that the photographs in Figure 7a–c display only microdischarges and not a combination of the two discharges. Comparing the barrier discharges generated in various ceramics, at the voltages slightly below the microdischarge onset, the light emission intensity increased with decreasing pore size. A particularly intense emission was observed for 2- $\mu\text{m}$  ceramics.

### 3. Optical Emission Characteristics

Emission spectroscopy is widely used for plasma diagnostics as a non-invasive and in situ method. It provides valuable information on excited atomic and molecular states, enables the determination of the rotational, vibrational, and electronic excitation temperatures of the plasma and thus the level of non-equilibrium, and the gas temperature. In addition, it enables the identification of many radicals and active atomic or molecular species, and so gives insight in the plasma chemical processes. We used emission spectroscopy to obtain information about excited species in the plasma and its level of non-equilibrium as a function of the discharge power and the gas composition.

The emission spectra gave us valuable information on excited atomic and molecular states and an insight into the plasma chemistry of the  $\text{N}_2$  and  $\text{O}_2$  mixtures. Figure 8 presents the emission spectra of microdischarges in the UV-VIS-NIR region taken at constant power in the mixtures with various contents of oxygen. In nitrogen-containing mixtures, the second positive system of  $\text{N}_2$  ( $\text{C}^3\Pi_u-\text{B}^3\Pi_g$ ), the first positive system of  $\text{N}_2$  ( $\text{B}^3\Pi_g-\text{A}^3\Sigma_u^+$ ), and atomic N and O lines were observed. Figure 9 and Figure 10 show the emission intensity of the  $\text{N}_2$  spectral band, and N and O lines as functions of the applied voltage and the oxygen content in the mixture, respectively. The increase of the emission intensity with the discharge power resulted from the increase of the number of discharge channels and the discharge current. Based on the spectral bands of the  $\text{N}_2$  second positive system, we were

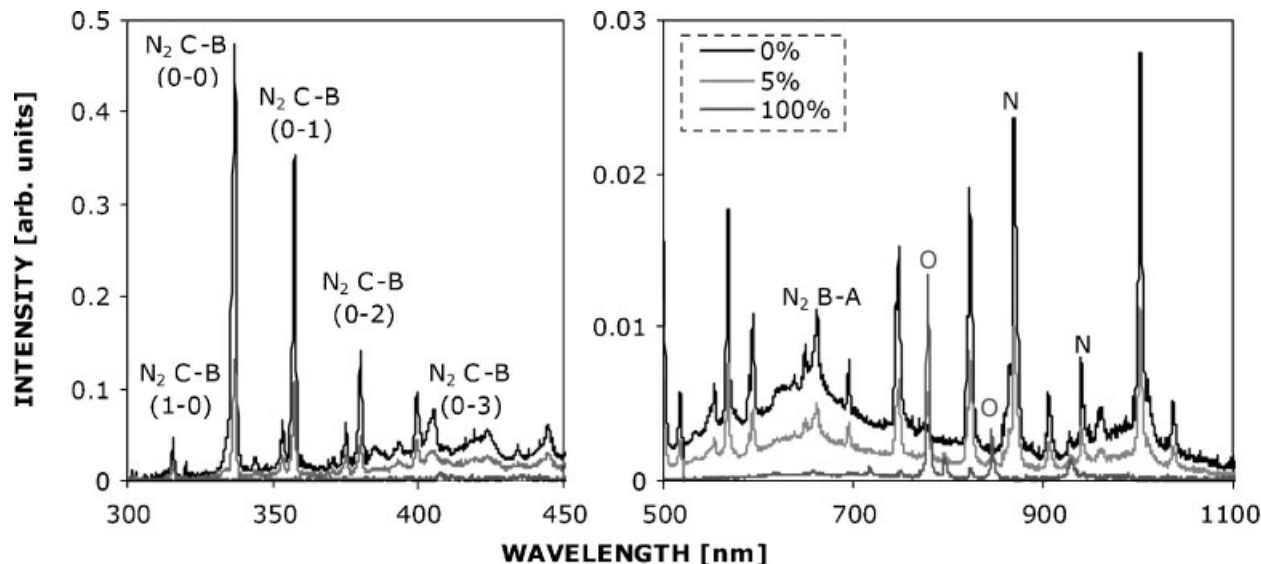


Figure 8. Emission spectra of microdischarges in the UV-VIS-NIR region in mixtures with various amounts of oxygen (pore size 80  $\mu\text{m}$ ,  $U=16.5$  kV).

able to determine rotational ( $T_r$ ) and vibrational ( $T_v$ ) temperatures by fitting the experimental spectra with the simulated ones using Specair software for spectral simulation.<sup>[14]</sup> Owing to fast collisional relaxation at atmospheric pressure, the gas temperature  $T_g$  equaled  $T_r$ . The temperatures measured in nitrogen/oxygen mixtures (pore size 80  $\mu\text{m}$ ,  $P=3-4$  W) gave the following results:

Pure  $\text{N}_2$ :  $T_g \approx T_r = 300 + 50$  K,  $T_v = 2\,000 \pm 300$  K

5%  $\text{O}_2$  in  $\text{N}_2$ :  $T_g \approx T_r = 350 \pm 50$  K,  $T_v = 2\,500 \pm 300$  K

20%  $\text{O}_2$  in  $\text{N}_2$ :  $T_g \approx T_r = 400 \pm 50$  K,  $T_v = 2\,800 \pm 300$  K

The accuracy of the  $T_r$  measurements was determined by the spectral resolution of our spectrometer. A vibrational

temperature  $T_v$  larger than  $T_r$  indicates non-equilibrium in the plasma, although  $T_v$  may not be well defined in strongly non-equilibrated conditions when vibrational states do not follow the Boltzmann distribution. The temperatures tend to increase with increasing oxygen concentration. As already discussed above, at a constant discharge power the number of discharge channels in oxygen was smaller when compared to the case for nitrogen. On the other hand, the amplitude of the pulses was higher so that the current carried by an individual discharge channel was also higher. Therefore, higher energy delivered in a single discharge channel gave correspondingly higher gas temperatures.

Many other unidentified bands have been observed in the spectra that probably result from the material of

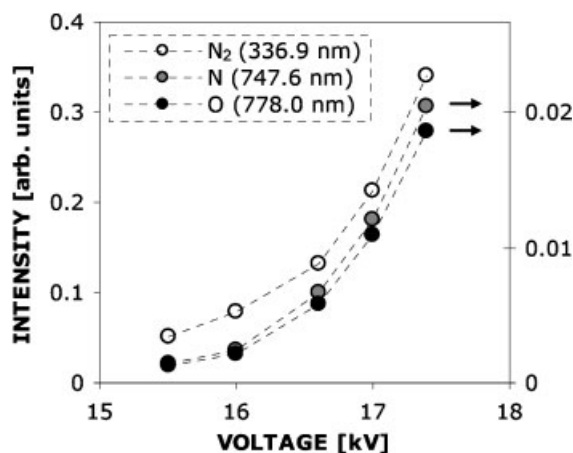


Figure 9. Emission intensity as a function of the applied voltage (pore size 80  $\mu\text{m}$ , 5%  $\text{O}_2$  in  $\text{N}_2$ ).

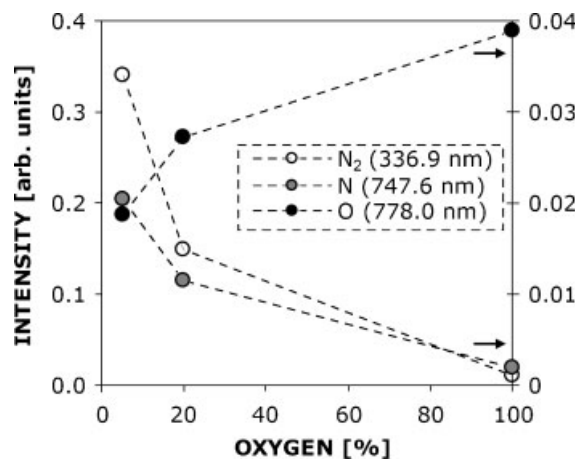


Figure 10. Emission intensity as a function of  $\text{O}_2$  concentration (pore size 80  $\mu\text{m}$ ,  $U=17.5$  kV).

the ceramics, which, besides alumina and silica, includes compounds containing Ca, Mg, and Na. Further investigation and interpretation of these bands are needed. Nevertheless, we observed no OH bands or H lines that are typically associated with water dissociation. We worked with dry synthetic gases. In addition, there was most likely no water adsorbed in the ceramics. However, the water effect must be investigated when testing practical applications, as it is present in real combustion exhaust.

#### 4. Theoretical Analysis of Discharge Mechanism

The mechanism of the microdischarges inside the porous ceramics is probably related to the back-corona discharge, a phenomenon often found in electrostatic precipitators.<sup>[15,16]</sup> It occurs when charged dielectric particles are collected on the electrode and form a porous layer of high resistivity, which the electric current must pass through. The highly resistive layer does not allow the charge to decay at the desired rate, resulting in a buildup of excess charge on the layer. When the voltage drop across the layer exceeds a critical value, an ultimate breakdown through the layer occurs. The breakdown occurs in the form of fine channels (microdischarges). Repetitive charge accumulations and subsequent breakdown of the dielectric layer result in regular pulsed microdischarges similar to what we observe in the porous ceramics. Back-corona discharge, however, does not occur only as microdischarges inside the dielectric layer, but also as surface barrier discharge propagating along the dielectric barrier. The current pulses and light emission of the microdischarges are much stronger compared to the diffuse homogeneous light of the surface barrier discharge.

The transition of the barrier discharge into a capillary discharge inside the ceramics is crucial for understanding the mechanism of the capillary microdischarges. Considering the geometry and the dimensions of the reactor, the discharge seems to be similar to micro-hollow cathode (MHC) or capillary plasma electrode (CPE) discharges.<sup>[17,18]</sup> In the case of the MHC discharge, the confinement of the microdischarges in small volumes is ruled by the White-Allis similarity law. The law relates the discharge-sustaining voltage  $U$  to the  $pd$  product and the ratio  $I/D$ , where  $p$ ,  $d$ ,  $I$ , and  $D$  are the pressure, the anode-cathode gap length, the discharge current, and the aperture of the cathode, respectively. In the MHC discharge, unlike in ceramics, the walls of the cavity are electrically conductive. The cathode fall region and corresponding parts of the discharge (e.g., positive column) may develop and result in the formation of the radial field inside the cathode cavity. This mechanism, however, is unable to proceed in the ceramic, which is a dielectric. No cathode fall can form inside the pores and no electric current can flow in the

radial direction. With respect to the geometry of the dielectric barrier between electrodes, our microdischarges are more similar to the CPE discharge, where dielectric capillaries cover one or both electrodes. Unfortunately, the basic properties of the CPE discharge have been subjected to few experimental studies and so the operating mechanisms of the CPE discharge are not well understood, and therefore particular comparison cannot be made.

The charge trapping on the cavity walls and the formation of the discharge inside very fine cavities is a phenomenon that also occurs in so-called ferroelectrets. Ferroelectrets are polymeric layers [e.g., poly(propylene), polyethylene, poly(tetrafluoroethylene)] of 10–100  $\mu\text{m}$  in thickness, with typical cavities of 10–100  $\mu\text{m}$  in diameter and 1–10  $\mu\text{m}$  in height, which are of particular interest due to their charge storage and electromechanical transducer properties.<sup>[19,20]</sup> By subjecting the layer to a high electric field, a Paschen's breakdown (microdischarge) inside the cavities is thought to be initiated, followed by a subsequent charge separation and charge trapping on the inner surfaces. The mechanism of the discharge formation inside the cavities of ferroelectrets is most likely different from the one inside the porous ceramics. Although a similar voltage is necessary to initiate the breakdown inside cavities of the ferroelectrets as inside the ceramics, our ceramics are, however, two to three orders of magnitude thicker. The energy of electrons in the ceramics is not sufficient to incorporate and store the charges inside such thick ceramics. In addition, the mechanical resistance of the ceramics is much better than that of organic polymer films.

To understand the physical mechanism of discharge in porous ceramics, we analyzed the transition of the barrier discharge into the capillary microdischarge inside the ceramics. Our analysis is based on the assumption that the charged particles of the barrier discharge can get inside pores only if their concentration reaches the value at which the Debye length  $h$  is smaller than the radius of the capillary (pore size)  $R$ , given as  $R = hQ$ , where  $Q$  is a constant. When the concentration of charge is small, the electrons inside the pore quickly diffuse out, leaving a negative space charge on the walls of the pore behind. This negative space charge restrains the entry of electrons from the barrier discharge inside the capillary. The exact description of entry of the electrons from the barrier discharge plasma into the capillary is very complicated. It requires tracking of the motion of charged particles, development of the geometry, the electric field intensity, and the space charge on the capillary walls. In that respect, a computer model developed by Kushner is appropriate.<sup>[21,22]</sup> Nevertheless, we tried to solve the problem in a simpler, although less accurate way.

Our approach is based on the analysis of the probability of sustaining a discharge inside a capillary in nitrogen. The

discharge plasma inside the capillary is quenched by an ambipolar diffusion of charged particles toward the walls of the capillary and the volume recombination of electrons and ions. The loss processes must be compensated by the electron-impact ionization in the volume of the capillary. According to Schottky's theory modified to include the volume recombination, the frequency of ionization  $\alpha$ , can then be expressed as:

$$\alpha = \frac{\rho_B^2 D_a}{R^2} + \beta n_0, \quad (1)$$

where  $\rho_B$ ,  $D_a$ ,  $R$ ,  $\beta$ , and  $n_0$  are the first zero of the Bessel function, the coefficient of ambipolar diffusion, the pore diameter, the coefficient of the volume recombination, and the concentration of charged particles at the pore axis, respectively.

As electrons move in a radial direction inside the capillary in a decelerating field (the walls of the capillary are negatively charged), their chaotic motion dominates, and can be described by the temperature  $T_e$ . Then the coefficient of the ambipolar diffusion can be expressed as:

$$D_a = \mu_+ \frac{kT_e}{e},$$

where  $\mu_+$ ,  $k$ , and  $e$  are the mobility of positive ions, Boltzmann's constant, and the elementary charge, respectively.

On the contrary, the strong electric field present in the axial direction promotes avalanche ionization and enables the discharge to enter the whole capillary. In the early stages of the breakdown, the electrons have highly coordinated velocities that dominate over the chaotic motion. Then the ionization frequency  $\alpha$  can be approximated by the first Townsend coefficient  $\delta$  and the electron drift velocity  $v_e$ :

$$\alpha = \delta v_e.$$

The electron drift velocity is a complicated function of the electric field  $E$ . We found data for nitrogen published by Huxley and Crompton<sup>[23]</sup> where  $v_e$  can be described by the following function for the reduced fields of 0.014–240 Td:

$$v_e = 1\,050 \frac{E}{N} \left( 0.75 + 38 \frac{0.9 + 7 \frac{E}{N} \sqrt{\frac{E}{N}}}{1 + 90 \left(\frac{E}{N}\right)^2} \right). \quad (2)$$

The first Townsend coefficient is a function of the reduced field strength  $E/p$ . Its generalized form is given by the semi-empirical expression:<sup>[24]</sup>

$$\frac{\delta}{p} = A \exp\left(-\frac{B}{E/p}\right), \quad (3)$$

where  $A$  and  $B$  are constants depending on the gas type and the electric field strength. We examined various values of  $A$  and  $B$  for different reduced field strengths, and other semi-empirical expressions and compared them with the experimental values from the literature.<sup>[25]</sup> We found the most favorable approximation when using the constants  $A = 8.8 \text{ cm}^{-1} \cdot \text{Torr}^{-1}$  and  $B = 275 \text{ V} \cdot \text{cm}^{-1} \cdot \text{Torr}^{-1}$ , which is optimal for the interval of  $27 < E/p < 200 \text{ V} \cdot \text{cm}^{-1} \cdot \text{Torr}^{-1}$ .

Finally, the values of the first Townsend coefficient were supplemented with the values of mobility and coefficient of recombination of positive ions ( $N_2^+$ ),  $\mu_{+0} = 2 \times 10^{-4} \text{ m}^2 \cdot \text{V}^{-1} \cdot \text{s}^{-1}$  (reduced value)<sup>[26]</sup> and  $\beta = 4.6 \times 10^{-14} \text{ m}^3 \cdot \text{s}^{-1}$  (for  $T_e \approx 10^4 \text{ K}$ ),<sup>[18,26]</sup> respectively, from the literature.

By substituting these expressions into Equation (1) we obtain the equation:

$$v_e \left(\frac{E}{p}\right) F\left(\frac{E}{p}\right) = \left(\rho_B^2 p \mu_+ + \beta Q^2 \frac{\varepsilon_0}{e} p\right) \frac{kT_e}{e} \frac{1}{(pR)^2}, \quad (4)$$

which relates the axial electric field  $E$  inside the capillary with the product of  $pR$  (or  $pD$  for pores in the ceramics, where  $D = 2R$ ). The concentration  $n_0$  was eliminated from the equation by the expression for the Debye length:

$$n_0 R^2 = \frac{\varepsilon_0 kT_e}{e^2} Q^2. \quad (5)$$

$E/p$  is a function of  $pR$  only if the volume recombination can be neglected. If the recombination is dominant, the reduced field is a function of  $\sqrt{pR}$ .

We tested several approximations of the electron drift velocity  $v_e$  and the first Townsend coefficient  $\delta/p$  for  $Q = 1$ ,  $p = 760 \text{ Torr}$ . We examined the electron drift velocity  $v_e$  for the condition of constant electron mobility, and, also given by Equation (2), for the first Townsend coefficient  $\delta/p$  expressed by Equation (3) and with various values for  $A$  and  $B$ .

Figure 11 shows the experimental data of the micro-discharge onset voltage, which were obtained by using the expression:

$$U_p = El = \frac{E}{p} pl, \quad (6)$$

where  $U_p$  is the voltage drop across the pore of length  $l$ , which in our case was identified as the thickness of the ceramics. Coming back to Equation (4) and (6), we can see that the voltage drop is a function of two variables:  $pR$  (or  $\sqrt{pR}$  when volume recombination dominates), and  $pl$ . Based on the various investigations of discharges in atmospheric pressure air and nitrogen, we assume  $T_e = 10^4 \text{ K}$ .<sup>[18]</sup> The experimental data gave the criteria for the approximation of the first Townsend coefficient  $\delta$ . With respect to the lack of experimental data for  $E/p$  less than  $25 \text{ V} \cdot \text{cm}^{-1}$ ,

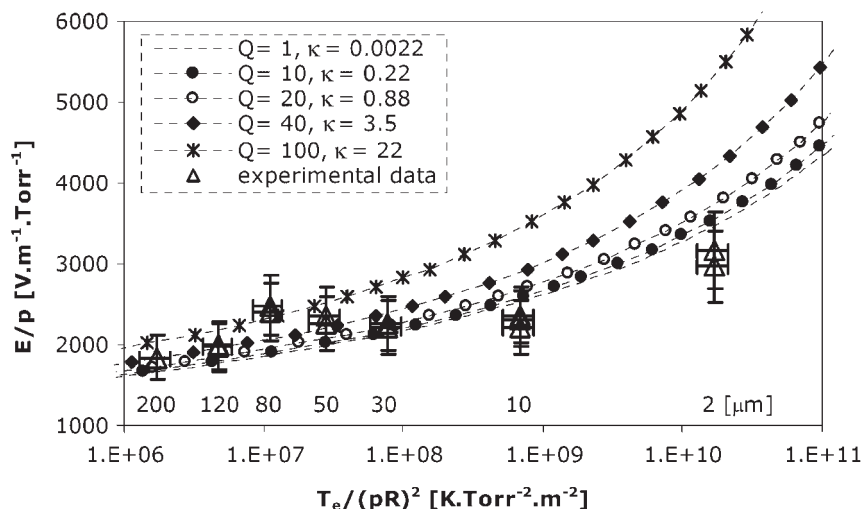


Figure 11. Comparison of the experimental values with theory for various values of  $Q$  and  $\kappa$ , in nitrogen. The effect of volume recombination is represented by dimensionless parameter  $\kappa$ . Numbers at the bottom of the figure (above x axis) represent the pore size of the ceramics.

the acceptable approximation is Equation (3) with the constants  $A = 8.8 \text{ cm}^{-1} \cdot \text{Torr}^{-1}$  and  $B = 275 \text{ V} \cdot \text{cm}^{-1} \cdot \text{Torr}^{-1}$ .

Figure 11 shows  $E/p$  as a function of the variable  $T_e/(pR)^2$  for various values of  $Q$  to test the effect of the ratio of the Debye length to the pore radius in the ceramics. We also calculated the value of the dimensionless parameter  $\kappa$ :

$$\kappa = \frac{\beta R^2 n_0}{\rho_B^2 D_a} = \frac{\beta \epsilon_0 p}{\rho_B^2 e p \mu_+} Q^2,$$

which represents the ratio between the losses of the charged particles by recombination and ambipolar diffusion to the capillary walls. For  $\kappa$  less than 1, volume recombination can be neglected. In Figure 11, the experimental data are displayed with errors bars. The accuracy of the  $U_p$  measurements was estimated to be  $\pm 15\%$ . A similar error was assumed for the pore size radius  $R$ , although this may be even bigger because we did not have exact data from the ceramics maker. The critical parameter is the geometry of the pores, which is far from the expected cylindrical geometry. This factor is not included in the error. The same applies to  $T_e$ , which we could not measure; in our case, we used  $10^4 \text{ K}$ , which is the generally accepted value typical of the atmospheric discharges in nitrogen or air. A 30% change of  $T_e$  has the same effect as a 15% change in  $R$ . We can conclude that within the considered errors, the described theory agrees with the experimentally measured data for  $Q < 20$ .

Theoretical analysis determined the condition under which transition of the barrier discharge into filamentary microdischarges inside porous ceramics may occur. It was shown that the concentration of the charges of the barrier discharge must reach a certain value so that the micro-

discharge can develop inside the pores. In addition, electron-impact ionization must dominate the loss processes by ambipolar diffusion and recombination inside the pores. Simplified theoretical analysis showed a good correlation with the experimentally measured data in nitrogen (Figure 11).

## 5. Technical Issues

We now consider two issues important for practical applications of the microdischarges generated inside the ceramics: the effect of the pressure drop and the discharge interaction with the ceramics.

From the point of view of industrial applications, such as exhaust gas treatment, the critical parameter is the pressure drop of the system. An excessive pressure drop may affect the

discharge characteristics and result in poor system performance and excessive energy consumption. Figure 12 shows the pressure drop across the ceramics as a function of the gas flow rate for various pore sizes. As the pore size decreased, the pressure drop increased exponentially. For pore sizes of 30–200  $\mu\text{m}$  and gas flow rates of 0.4 and 2.0  $\text{L} \cdot \text{min}^{-1}$ , the pressure drop ranged from 0.1 to 0.8 kPa, respectively. Pressure drops smaller than 1 kPa are usually acceptable in most industrial applications. On the other hand, high pressure drop was observed for the of 2- and 10- $\mu\text{m}$  ceramics, equal to 20 and 4.5 kPa, respectively, even at the lowest gas flow rate (0.4  $\text{L} \cdot \text{min}^{-1}$ ). With increasing gas flow rate, the surface of the ceramics should be correspondingly enlarged to keep the pressure

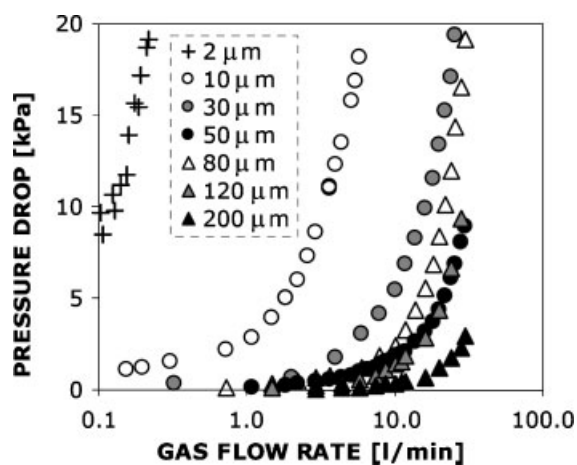


Figure 12. Pressure drop across the ceramics as a function of gas flow rate for various pore sizes.

drop constant. The increase of the gas flow rate slightly increased the onset voltage of the microdischarges. For a given voltage, the current decreased with the gas flow rate because the discharge was quenched by the gas flowing at high speed through the ceramics pores.

When dealing with the discharges generated on the surfaces and inside the ceramics, plasma–surface interaction and erosion of the material may become an important issue. Several papers describe the interaction of the filamentary microdischarges with electrodes or dielectrics that result in production of particles/aerosols by various physical and chemical routes.<sup>[27,28]</sup> Surface erosion has to be particularly taken into account when dealing with catalyst supported on dielectric surfaces. In order to examine the erosion of ceramics caused by the discharge action, a test with porous ceramics impregnated with TiO<sub>2</sub> catalyst (pore size 80 μm) was performed. Operating the discharge at a power of about 8 W for 5 min, we confirmed deposition of the catalyst on the mesh electrodes and the inner walls of the reactor. We performed similar tests with the ceramics without the catalyst and found no deposits, even after 10 h of operation. We also examined the mechanical changes by comparing the pressure drop versus the gas flow characteristics before and after the test and found no difference. Therefore, we presume that erosion of the ceramics (without a catalyst) is a very slow process.

Nevertheless, we found more significant erosion of the ceramics in DC microdischarges. By applying DC power, the charges are accumulated on only one surface and the probabilities of permanent (non-pulsating) breakdown and subsequent mechanical damage of the ceramics are high. An alternative charging and discharging of the ceramics surface by the applied harmonic voltage in AC power is better, which is the primary advantage over the use of DC. The study of DC discharge also showed that by increasing thickness of the ceramics by a factor of two, the onset voltage nearly doubled. Therefore, with respect to prospective applications, instead of increasing the thickness of the porous ceramics, it is preferable to increase the surface of the ceramics or to use several reactors in parallel.

## Conclusion

Electrical and optical properties of microdischarges generated inside porous ceramics by AC high voltage power were investigated. The effects of the pore size, discharge power, and gas mixture on the discharge properties and development were described. It was found that the onset voltage of the microdischarges decreased with pore size, while the slope of the *P/U* characteristics increased with pore size. The amplitude of the current pulses increased with the applied voltage, the pore size, and oxygen contents. In nitrogen, the light emission was relatively homogeneously distributed over the whole surface of the

ceramics, especially for pore sizes of 50 and 80 μm. On the other hand, in air or oxygen, the microdischarges concentrated mainly at the circumference of the ceramics, and the total discharge power decreased while the amplitude of the pulses increased. Emission spectroscopy also showed changes in the emission spectra depending on the content of oxygen. The presence of the N<sub>2</sub> systems and atomic N and O lines indicated relatively cold plasma (300–500 K) with a high level of non-equilibrium.

Theoretical analysis of the microdischarge mechanism addressed the transition of the surface barrier discharge mode into the capillary microdischarge mode, with respect to the pore size, considering the effect of charge transfer into the pores and the role of ambipolar diffusion. Plasma–surface interaction of the microdischarges with the ceramics did not seem to deteriorate the ceramics properties; no erosion or pressure drop change was observed. Overall, optimal generation of the microdischarges and their distribution in the ceramics were observed especially for the ceramics with pore sizes of 50 and 80 μm. Microdischarge formation inside porous ceramics represents a novel way to generate large-volume, stable atmospheric-pressure plasmas. In addition, by loading the ceramics with a catalyst, such hybrid plasma-catalyst system may be significantly effective for flue gas treatment.

**Acknowledgements:** This research was supported by the *Slovak Research and Development Agency* through grants APVT 20-032404 and SK-FR-00506, and by the *Slovak Grant Agency* through grant 1/3041/06.

Received: February 28, 2007; Revised: June 11, 2007; Accepted: June 28, 2007; DOI: 10.1002/ppap.200700022

**Keywords:** AC barrier discharges; microdischarges; optical emission; porous ceramics

- [1] T. Oda, T. Kato, T. Takahashi, K. Shimizu, *IEEE Trans. Ind. Appl.* **1998**, *34*, 268.
- [2] T. Yamamoto, M. Okubo, T. Nagaoka, K. Hayakawa, *IEEE Trans. Ind. Appl.* **2002**, *38*, 1168.
- [3] H.-H. Kim, G. Prieto, K. Takashima, S. Katsura, A. Mizuno, *J. Electrostat.* **2002**, *55*, 25.
- [4] T. Hammer, *Plasma Sources Sci. Technol.* **2002**, *11*, 1.
- [5] F. Holzer, U. Roland, F.-D. Kopinke, *Appl. Catal. B: Environ.* **2002**, *38*, 163.
- [6] H.-H. Kim, *Plasma Process. Polym.* **2004**, *1*, 91.
- [7] B. M. Penetrante, M. C. Hsiao, J. N. Bardsley, *Plasma Sources Sci. Technol.* **1997**, *6*, 251.
- [8] M. Kraus, B. Eliasson, U. Kogelschatz, A. Wokaun, *Chem. Phys. Chem.* **2001**, *3*, 294.
- [9] N. Blin-Simian, P. Tardiveau, A. Risacher, F. Jorand, S. Pasquiers, *Plasma Process. Polym.* **2005**, *2*, 256.
- [10] N. Jidenko, M. Petit, J.-P. Borra, *J. Phys. D: Appl. Phys.* **2006**, *39*, 281.
- [11] K. Hensel, S. Katsura, A. Mizuno, *IEEE Trans. Plasma Sci.* **2005**, *33*, 574.
- [12] K. Hensel, Y. Matsui, S. Katsura, A. Mizuno, *Czech. J. Phys.* **2004**, *54*, C683.

- [13] J. Sawada, Y. Matsui, K. Hensel, I. Koyamoto, K. Takashima, S. Katsura, A. Mizuno, *Proc. Int. Conf. Appl. Electrostat.* **2004**, 5, 128.
- [14] C. O. Laux, T. G. Spence, C. H. Kruger, R. N. Zare, *Plasma Sources Sci. Technol.* **2003**, 12, 125.
- [15] A. Mizuno, *IEEE Trans. Dielec. Electr. Insul.* **2000**, 7, 615.
- [16] A. Jaworek, A. Krupa, T. Czech, *J. Phys. D: Appl. Phys.* **1996**, 29, 2439.
- [17] K. H. Becker, K. H. Schoenbach, J. G. Eden, *J. Phys. D: Appl. Phys.* **2006**, 39, R55.
- [18] K. H. Becker, U. Kogelschatz, K. H. Schoenbach, R. J. Barker, *“Non-Equilibrium Air Plasmas at Atmospheric Pressure”*, Institute of Physics Publishing, Bristol 2005.
- [19] M. Wegener, W. Wirges, J. Fohlmeister, B. Tiersch, R. Gerhard-Multhaupt, *J. Phys. D: Appl. Phys.* **2004**, 37, 623.
- [20] A. Mellinger, *PhD Thesis*, University of Potsdam, 2004.
- [21] M. J. Kushner, *J. Appl. Phys.* **2004**, 95, 846.
- [22] M. J. Kushner, *J. Phys. D: Appl. Phys.* **2005**, 38, 1633.
- [23] L. G. H. Huxley, B. W. Crompton, *“The Diffusion and Drift of Electrons in Gases”*, Wiley-Interscience, New York 1974.
- [24] S. C. Brown, *“Basic Data of Plasma Physics”*, Wiley-Interscience, New York 1959.
- [25] V. L. Granovskiy, *“Electric Current in Gas”* (in Russian), Nauka, Moscow 1971.
- [26] B. M. Smirnov, *“Ions and Excited Atoms in a Plasma”* (in Russian), Atomizdat, Moscow 1974.
- [27] J.-P. Borra, *J. Phys. D: Appl. Phys.* **2006**, 39, R19.
- [28] T. Yamamoto, B. W. L. Jang, *IEEE Trans. Ind. Appl.* **1999**, 35, 736.